Supporting information

Enhanced magnetic properties and thermal stability of highly ordered ε-Fe_3N_{1+x} ($-0.12 \leq x \leq -0.01$) nanoparticles

Yong Li,[†] Desheng Pan,[†] Yangtao Zhou,[†] Qifeng Kuang, [†] Chinwei Wang,[‡] Bing Li,[†] Bingsen Zhang,[†] Jihoon Park,[§] Da Li,*[,†] Chuljin Choi*[,§] and Zhidong Zhang[†]

[†]Shenyang National Laboratory for Materials Science, Institute of Metal Research, and School of Material Science and Engineering, University of Science and Technology of China, Chinese Academy of Sciences, 72 Wenhua Road, Shenyang, 110016, China

[‡]National Synchrotron Radiation Research Center, Hsinchu, 30076, Taiwan

[§]Korea Institute of Materials Science, 797 Changwondaero, Seongsangu, Changwon, Gyeongnam, 51508, Korea

Table S1. Summary of carbon coated Fe_3N_{1+x} nanoparticles prepared with varying the amount of OLA, the catalyst, the reaction temperature (T)/time (t), and the heat-treatment conditions.

TEPA/mL		60					
$Fe(acac)_2$/mmol		2					
OLA/mL		15	15	30	45	30	
$Pt(acac)_2$/mmol		0.025					
Reaction T/K		533				553	
Reaction t/h		5				5	
Synthetic products	Fe_3N	√	√	√	√	√	
	Fe		√	√	√	√	
	Fe_3O_4					√	
Mass/g		~0.1				6 (multiple for large scale)	
Heat-treatment	T/K	800				720	800
	t/min	1					
Annealed samples	Fe_3N_{1+x}	√	√	√	√	√	√
	Fe_3C					√	√
	Fe_3O_4					√	√

A checkmark denotes the primary component in the synthetic products and the annealed samples. Carbon served as the shells is not indicated for clarity. A green box indicates the presence of single phase Fe_3N_{1+x} nanoparticles, as determined by the powder XRD and TEM. The blue boxes indicate the presence of a main phase of Fe_3N_{1+x} and a small amount of impurities Fe_3C and Fe_3O_4.

Table S2. Technical data of Rietveld refinements of NPD data for the S1, S2 and S3 samples with different magnetic structure in a temperature (T) range of 300 and 650 K.

sample		S1	S2	S3				
T (K)		300	300	300	450	500	600	650
m//c	χ^2	3.89	9.68	2.31	3.29	3.55	3.29	5.10
	Bragg R-factor	0.96	1.88	1.741	1.670	1.860	1.867	2.540
	R_f-factor	0.938	1.75	1.660	1.523	1.699	1.960	2.743
	Magnetic R-factor	2.87	4.51	4.318	4.031	5.695	9.688	-
m⊥c	χ^2			2.34	3.20	3.45	3.19	-
	Bragg R-factor			1.594	1.498	1.484	1.529	-
	R_f-factor			1.623	1.390	1.528	1.824	-
	Magnetic R-factor			5.308	4.975	4.520	4.990	-

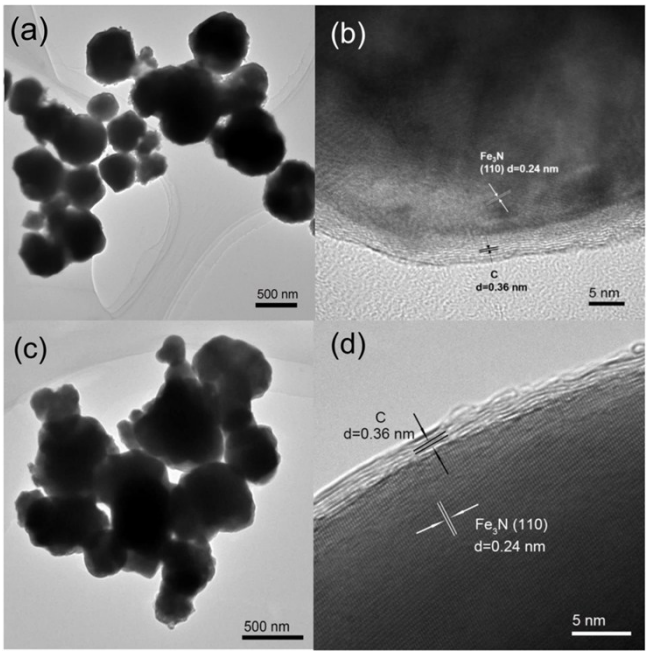

Figure S1. TEM and HRTEM images of (a, b) the pristine carbon coated ε-Fe_3N/Fe nanoparticles synthesized with 15 mL of OLA and (c, d) the carbon coated ε-$Fe_3N_{0.88}$ nanoparticles obtained by annealing at 800 K for 1 min.

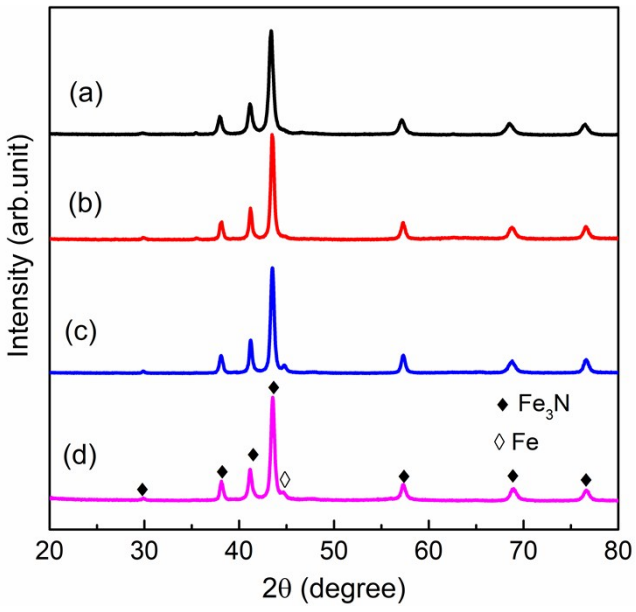

Figure S2. XRD patterns of the as-synthetic carbon coated Fe/Fe_3N nanoparticles synthesized with (a) 0.025 mmol of $Pt(acac)_2$ and 15 mL of OLA, (b) 45 mL of OLA , (c) 30 mL of OLA, (d) 15 mL of OLA at a reaction temperature of 533 K. The XRD patterns indicate that all the products consist of ε-Fe_3N and a small amount of Fe. The amount of Fe can be tuned by $Pt(acac)_2$ and surfactant of OLA.

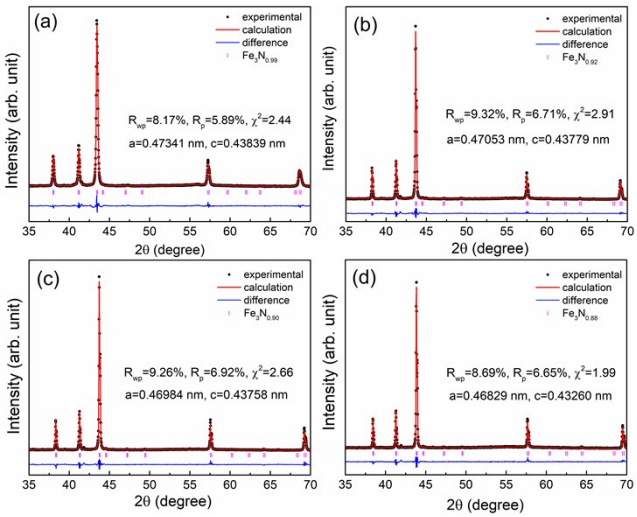

Figure S3. Powder XRD patterns of (a) carbon coated ε-$Fe_3N_{0.99}$, (b) carbon coated ε-$Fe_3N_{0.92}$, (c) carbon coated ε-$Fe_3N_{0.90}$ and (d) carbon coated ε-$Fe_3N_{0.88}$ nanoparticles for the experimental data recorded at room temperature (solid dot) with Rietveld refinements and difference. All Bragg diffraction peaks match with the hcp ε-Fe_3N_{1+x} in a space group $P6_322$. Calculated R factors and lattice parameters were presented in the figures.

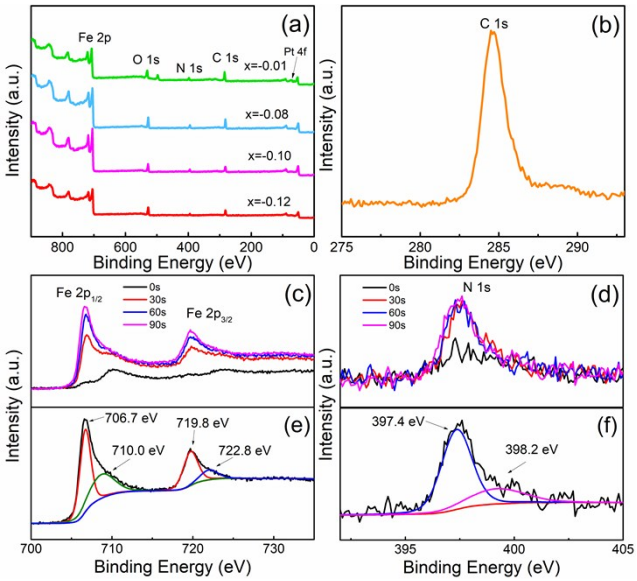

Figure S4. (a) XPS survey spectra of the carbon coated ε-Fe_3N_{1+x} nanoparticles with different x values. (b) C 1s spectrum of the surface of carbon coated ε-$Fe_3N_{0.88}$ nanoparticles. The binding energy at 285 eV in the C1s spectrum indicates that carbon exists on the surface of ε-$Fe_3N_{0.88}$ nanoparticles. (c) Fe 2p and (d) N 1s XPS spectra of carbon coated ε-$Fe_3N_{0.88}$ nanoparticles with the surface sputtered for 0 s, 30 s, 60 s, and 90 s, respectively. Fitting XPS spectrum of (e) Fe 2p and (f) N 1s recorded at a sputtering time of 90 s. The binding energy peaks at 706.7 eV and 719.8 eV are assigned to the Fe-N covalent bond of our ε-$Fe_3N_{0.88}$, while those at 710.0 eV and 722.8 eV are assigned to Fe oxides. The binding energy peak at 397.4 eV is assigned

to the N element in ε-$Fe_3N_{0.88}$, while that at 398.2 eV is assigned to the C-N. Element composition and quantitative analysis of Fe and N in the ε-phases can be investigated by peak fitting procedure, according to the formula $C_x = (I_x/S_x)/(\sum I_i/S_i)$, where C_x is the atomic percent, I_x the area, and S_x the sensitive factor.[1]

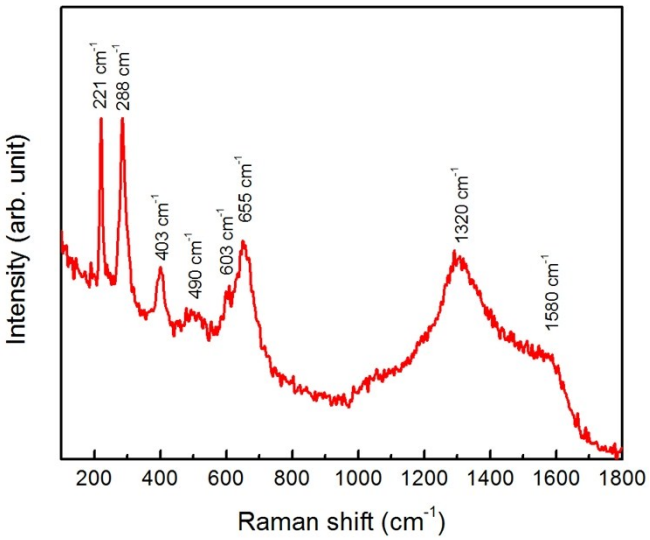

Figure S5. Raman spectrum of the carbon coated ε-$Fe_3N_{0.88}$ nanoparticles. Raman analysis is an effective method to characterize iron oxides and carbon in the iron oxide and carbon composite.[2] Figure S5 shows the presence of bands at 220 cm^{-1}, 288 cm^{-1}, 403 cm^{-1}, 490 cm^{-1}, 603 cm^{-1} and 655 cm^{-1} below 1000 cm^{-1} and two broad bands with the peak at 1320 cm^{-1} and 1580 cm^{-1}, respectively. Because of Raman experiment on the nanoparticles conducted in air and using 65 mW of laser power at 633 nm, the Fe_3O_4 may undergo laser-induced degradation to α-Fe_2O_3.[3] Among these the band at 655 cm^{-1} is assigned to Fe_3O_4, while other bands around 220 cm^{-1}, 288 cm^{-1}, 403 cm^{-1}, 490 cm^{-1}, 603 cm^{-1} and 1320 cm^{-1} may correspond to α-Fe_2O_3.[2-4] No band at around 700 cm^{-1} shows the absence of γ-Fe_2O_3. Similar to the previous Raman spectrum for Fe_3O_4/C,[2] the two broad bands with the peaks at 1320 cm^{-1} and 1580 cm^{-1} should be characteristic of the D band and G band for carbon. It is in good agreement with the result that carbon shells are present on the surfaces of ε-Fe_3N_{1+x} nanoparticles (Figure S1 and Figure S4).

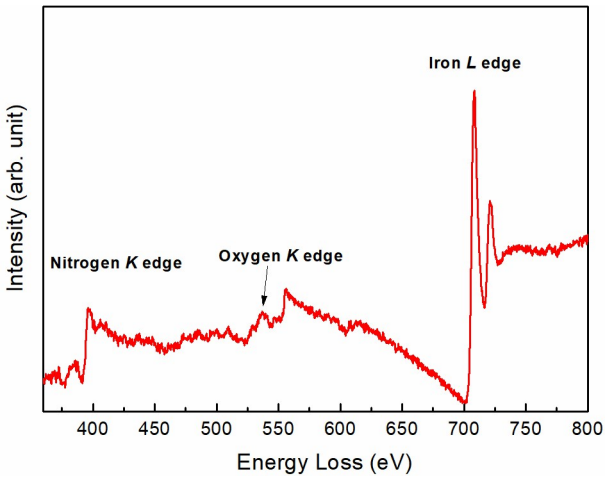

Figure S6. Full range of EELS spectra of the carbon coated ε-$Fe_3N_{0.88}$. A relative lower intensity of oxygen element than those of N and Fe elements is observed from the full range of EELS spectrum recorded on the carbon coated ε-$Fe_3N_{0.88}$ nanoparticles, indicating a small amount of oxygen in the presence of the carbon coated ε-Fe_3N_{1+x} nanoparticles.

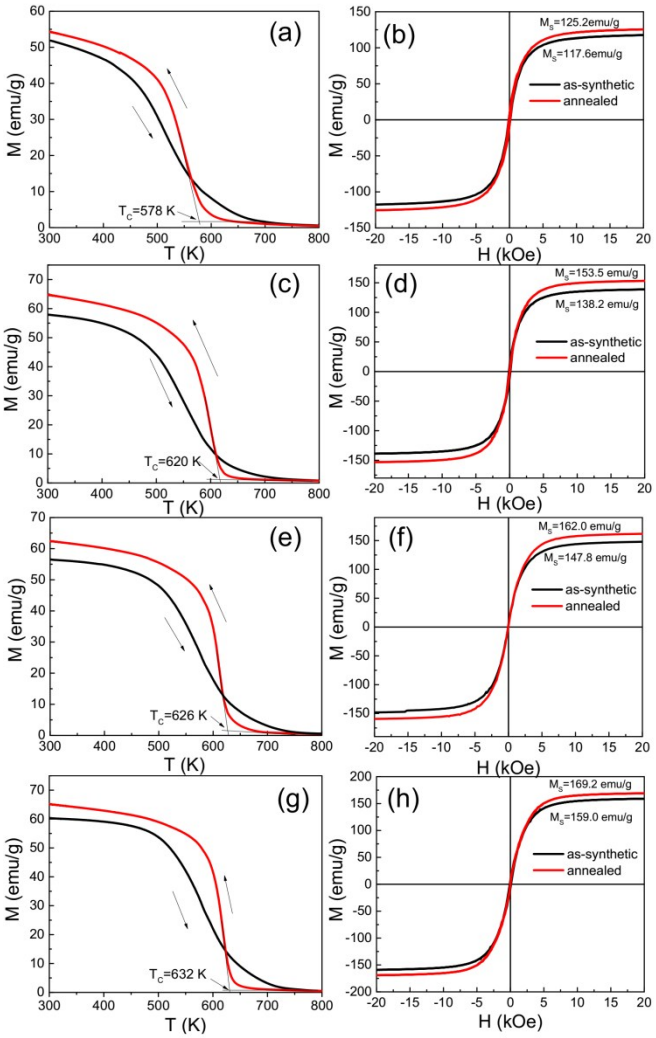

Figure S7. Temperature dependence of magnetization (MT) and room-temperature hysteresis loop of the pristine products synthesized with (a, b) 0.025 mmol of $Pt(acac)_2$ and 15 mL of OLA, (c, d) 45 mL of OLA, (e, f) 30 mL of OLA, (g, h) 15 mL of OLA at a reaction temperature 533 K. Temperature dependence of magnetization was recorded from the warming and the cooling processes in a temperature range between 300 K and 800 K.

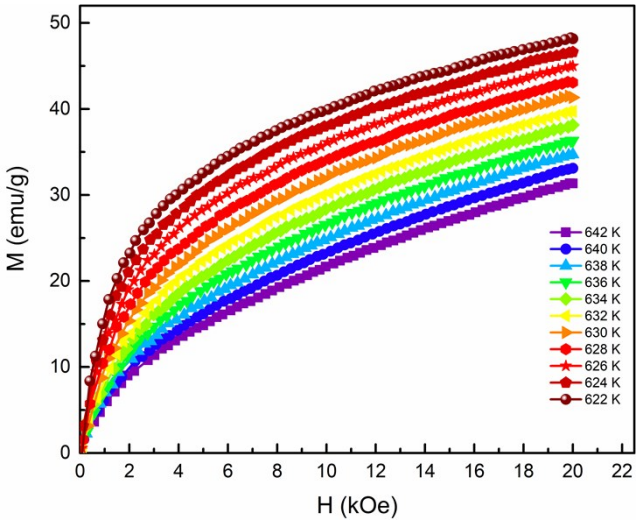

Figure S8. Isothermal magnetization curves of the carbon coated ε-$Fe_3N_{0.88}$ nanoparticles measured at different temperatures.

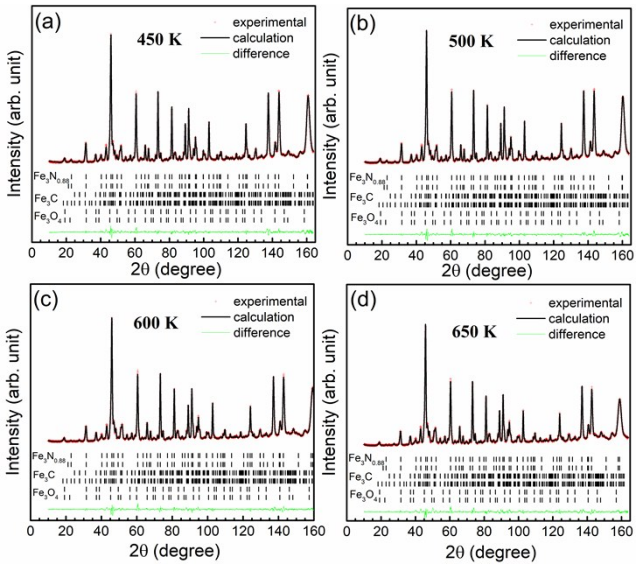

Figure S9. NPD data for the S3 sample recorded at (a) 450 K, (b) 500 K, (c) 550 K and (d) 650 K (solid crosses) with Rietveld refinements and difference curves. Taking account of a small amount of impurities (Fe_3O_4 and Fe_3C), the refinements of the NPD data for ε-Fe_3N_{1+x} were carried out based on an hcp crystal structure in a space group $P6_322$ and a magnetic structure with the m//c mode. The refinements with a magnetic structure with the m perpendicular to the c axis are not shown here.

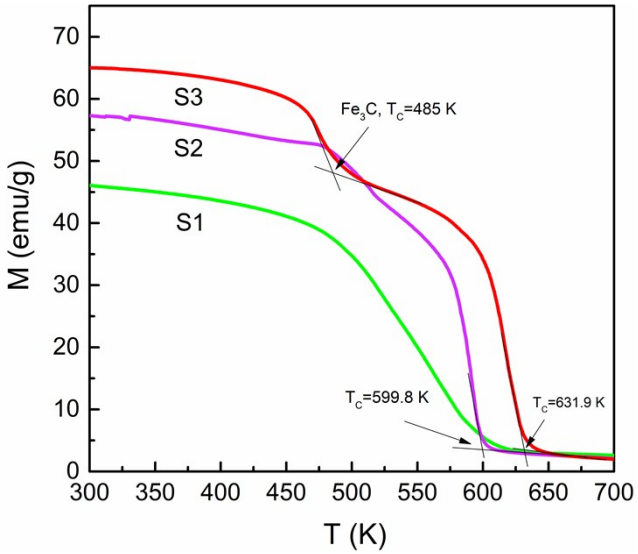

Figure S10. Magnetization as a function of temperature for the S1, S2 and S3 samples in a warming process measured in a magnetic field of 1 kOe. It reveals a broad magnetic transition for the S1 sample, possibly due to diffusion reaction between Fe and Fe_3N. As a result, an obvious increase in T_C is presented in the ε-iron nitrides in the S2 and S3 samples. The T_C is about 600 K for S2 and 631.9 K for S3, respectively. The kink around 485 K in the MT curve of S3 is attributed to the ferromagnetic-paramagnetic transition of Fe_3C.

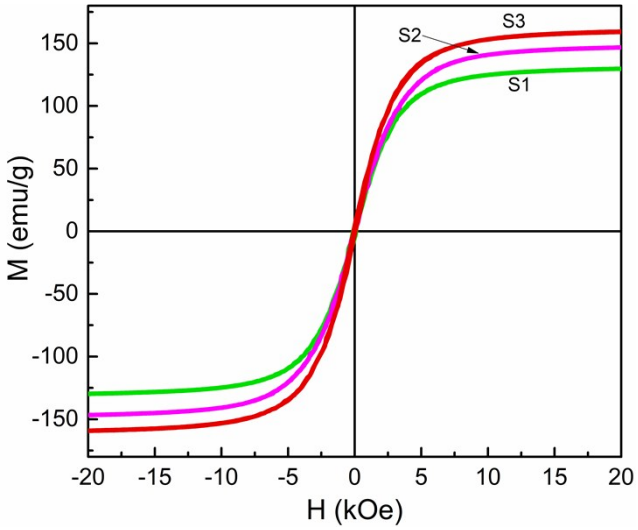

Figure S11. Room-temperature hysteresis loops of the S1, S2 and S3 samples. It shows an increase in the saturation magnetization M_S in an order of S1, S2, and S3.

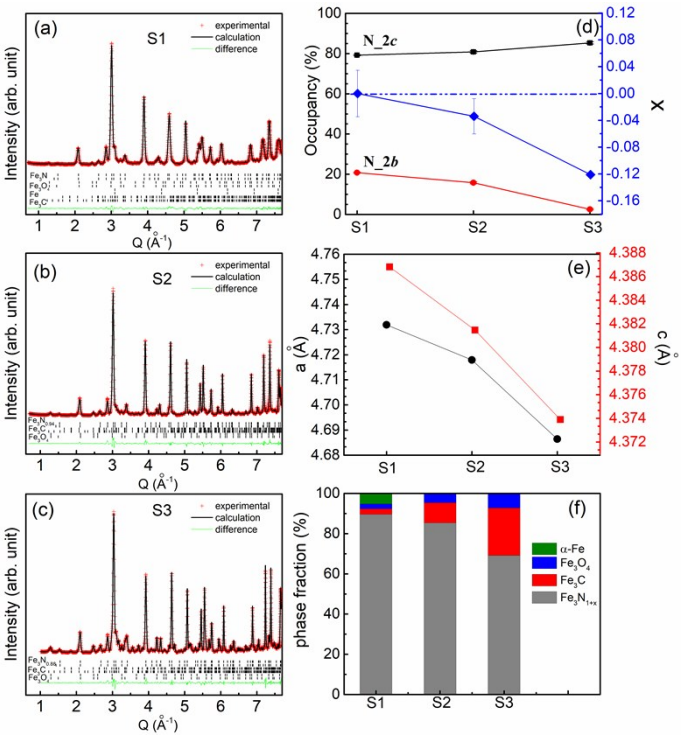

Figure S12. NPD data for (a) S1, (b) S2 and (c) S3 recorded at 300 K (solid crosses) with Rietveld refinements and difference curves. (d) Phase fraction, (e) lattice parameters *a* and *c*, (f) x value and N occupancy of ε-iron nitride in the S1, S2 and S3.

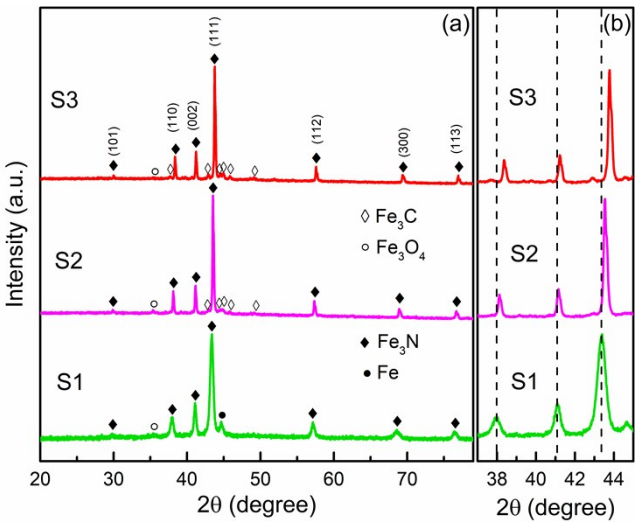

Figure S13. (a) Powder XRD patterns of the S1, S2 and S3. (b) Enlarged powder XRD patterns of S1, S2 and S3 at low 2θ values. Compared with the pristine ε-Fe_3N in the S1, the widths of the XRD peaks for the annealed ε-Fe_3N_{1+x} become narrow, indicating an improved crystallization of the S2 and S3 samples, while the shift of the XRD peaks to high 2θ angles reveals a lattice contraction due to decrease of the nitrogen content. Only one ε-iron nitride emerged in the S2 and S3 further illustrates that the ε-Fe_3N_{1+x} are stable and heat treatment at a temperature below 800 K did not result in thermal decomposition to form Fe and other iron-nitrides.

1. J.F. Moulder, W. F. S., P.E. Sobol, K.D. Bomben, in: J. Chastain (Ed.), Handbook of X-ray Photoelectron Spectroscopy, Perkin-Elmer Corporation, Physical Electronics Division, EdenPrairie, MN. **1992**, 25, 55-81, 83, 85.
2. K. Song, Y. Lee, M.R. Jo, K. M. Nam, Y.M. Kang, Nanotechnology 23 (2012) 505401.
3. O. N. Shebanova, P. Lazor, Journal of Solid State Chemistry 174 (2003) 424–430.
4. K. S. K. Varadwaj, M.K. Panigrahi, J. Ghose, Journal of Solid State Chemistry 177 (2004) 4286–4292.